Solution Combustion Synthesis and Energy Transfer in $LaMgAl_{11}O_{19}:Tb^{3+}/Sm^{3+}$ Tunable Phosphor

S.P. Puppalwar[1,*], M.S. Mendhe[1], S.J. Dhoble[2]

[1]Department of Physics, Kamla Nehru Mahavidyalaya, Nagpur 440009, India
[2]Department of Physics, R.T.M. Nagpur University, Nagpur 440033, India

*Corresponding author: E-mail: suresh.puppalwar@gmail.com; Tel.: (+91) 9881049243

DOI: 10.5185/amlett.2021.021601

Tb^{3+}/Sm^{3+} single as well as co-doped $LaMgAl_{11}O_{19}$ (LMA) phosphors have been synthesized by a low-temperature solution combustion method. The X-ray diffraction pattern, photoluminescence properties and energy transfer (ET) processes between rare earth (RE) ions, were investigated in detail. The mechanism of energy transfer (ET) from Tb^{3+} to Sm^{3+} was seen as the dipole–dipole interaction. Efficient ET from Tb^{3+} to Sm^{3+} ions was observed, leading to color-tunable emissions of LMA:0.02Tb^{3+}, x Sm^{3+} (x = 0.005 to 0.02 mol) phosphors. The efficiency of the ET gradually increased with increase in the Sm^{3+} ion concentration, reaching a maximum of 78.28% at Tb^{3+} ion concentration 0.02mol. The critical distance (R_c) among sensitizer and activator by the concentration quenching method was estimated to be 27.96 Å. The LMA: Tb^{3+}, Sm^{3+} phosphors exhibited the emission peaks in the blue ($^5D_3 \rightarrow {}^7F_{J\,=\,5,\,4,\,3,\,\text{and}\,2}$), green ($^5D_4 \rightarrow {}^7F_{J\,=\,6,\,5,\,\text{and}\,4}$), and orange-red ($^4G_{5/2} \rightarrow {}^6H_{J\,=\,5/2,\,7/2,\,\text{and}\,9/2}$) regions under the excitation wavelength of 375 nm. As a consequence of fine-tuning of the emission composition of the Tb^{3+} and Sm^{3+} ions, multicolor emitting luminescence properties can be achieved in a single host lattice LMA.

Introduction

The trivalent rare earth (RE) ions (Eu^{3+}, Yb^{3+}, Ho^{3+}, Dy^{3+}, Nd^{3+}, Tb^{3+}, Ce^{3+}, Sm^{3+}, Er^{3+}, Tm^{3+} etc) have been considered as one of the most appropriate candidates for multicolor light emission and even white light emission when they are incorporated into the host matrix. The trivalent RE ions doped phosphors have been gaining importance in recent years due to their fascinating optical properties and the great variety of applications. In optical materials, fluorescence efficiency is the most crucial and significant parameter for their optical applications. In single RE ion doped materials, increase the fluorescence efficiency by increasing the dopant concentration up to appropriate value and then they might be decreased due to concentration quenching effect [**1**]. To avoid this problem and to yield fruitful results, energy transfer (ET) process between multi-activators is being tried in optical materials. ET process not only improves the fluorescence efficiency but also helpful to adjust the relative intensities of activators. Due to this crucial phenomenon, ET process has become an attractive subject to achieve color-tunable emission or multicolor phosphors during the past decades. Consequently, possible ET process among RE combinations in various materials have been reported earlier, especially $Ce^{3+} \rightarrow Tb^{3+}$, $Tb^{3+} \rightarrow Sm^{3+}$, $Tb^{3+} \rightarrow Eu^{3+}$, $Sm^{3+} \rightarrow Eu^{3+}$, $Dy^{3+} \rightarrow Sm^{3+}$ etc. [**2-11**]. ET mechanism in potassium-fluoro-phosphate glasses has been investigated for Tb^{3+}-Sm^{3+} pair [**12**]. Li *et. al.*, reported the recent development in phosphors with different emitting colors via ET [**13**]. Recently, our previous work [**14,15**] reported an efficient ET from Ce^{3+} to Tb^{3+} in $SrYAl_3O_7$ and Tb^{3+} to Eu^{3+} in $CaLaAlO_4$ phosphors.

It is well known that the $^5D_4 \rightarrow {}^7F_J$ (J = 6, 5, and 4) characteristic emissions of Tb^{3+} ions are mostly in the green region while the $^4G_{5/2} \rightarrow {}^6H_{J/2}$ (J = 5, 7, and 9) characteristic emissions of Sm^{3+} ions are mostly in the orange region. At an appropriate concentration of Sm^{3+} ions, the fluorescence efficiency of the Sm^{3+} single doped phosphors might be decreased due to concentration quenching effect. Due to this fluorescence efficiency in orange region of Sm^{3+} doped phosphors is require to increased by secondary RE dopant ion. Tb^{3+} is one of the best secondary RE dopant ions which increased the fluorescence efficiency of Sm^{3+} doped phosphors [**16-18**].

The $LaMgAl_{11}O_{19}$ (LMA) lattice belongs to hexagonal of magnetoplumbite-type structure and has attracted much attention due to its excellent chemical and luminescent properties. Synthesis and luminescent properties of orange-red emitting phosphor $LaMgAl_{11}O_{19}:Sm^{3+}$ was reported by Min et al. in 2014 [**19**]; and also reported that the $LaMgAl_{11}O_{19}:Sm^{3+}$, Eu^{3+} was one of the promising red-emitting phosphor for solar cells and near-ultraviolet white light-emitting diodes [**20**]. To the best of our knowledge, synthesis and photoluminescence (PL) properties of Tb^{3+}/Sm^{3+} co-doped $LaMgAl_{11}O_{19}$ (LMA) phosphors have not been reported. In present work, we choose LMA as a host while Tb^{3+} and Sm^{3+} ions as activators to synthesize a series of LMA: Tb^{3+}/Sm^{3+} phosphors through low-temperature solution combustion method. Tb^{3+} has been taken as sensitizing ion and Sm^{3+} as activator ion. We have also reported here the structural and photoluminescence properties of the prepared phosphors. Furthermore, the ET from the Tb^{3+} to Sm^{3+} ions and dipole-dipole interaction responsible for ET process has been also discussed in details.

Experimental

Materials details

In the present study, low-temperature solution combustion technique by using urea has been employed for the synthesis of Tb^{3+}/Sm^{3+} single as well as co-doped $LaMgAl_{11}O_{19}$ phosphors. The precursors: Lanthanum nitrate [$La(NO_3)_3.6H_2O$], Magnesium nitrate [$Mg(NO_3)_2.6H_2O$], Aluminum nitrate [$Al(NO_3)_2.9H_2O$], Urea [NH_2CONH_2], (all A.R. grade of 99.99 purity – E. Merck) and Terbium nitrate [$Tb(NO_3)_3.6H_2O$], Samarium oxide [Sm_2O_3] (both rare earths 99.99% purity - Loba), where metal nitrates are used as oxidizer and urea as a fuel. All these were weighed according to the desired stoichiometric ratio. The heat of combustion is maximum for O/F ratio equal to1 [**21**]. Nitrate form of Samarium was obtained by dissolving the Sm_2O_3 into diluted nitric acid and warming these solutions at 50–60 °C for 10–15 min.

Material synthesis

For the synthesis of $LaMgAl_{11}O_{19}$:Tb, Sm, stoichiometric amount of the all reactants lanthanum nitrate, magnesium nitrate, aluminium nitrate, terbium nitrate, prepared nitrate form of samarium and urea were dissolved in 150 ml of H_2O in a 250 ml beaker. The solution was stirred for 30 min and then kept on a magnetic stirrer for 10–20 minutes at 80–100 °C to get uniform mixing and after evaporation of water it get converted into the gel of precursors. This gel in beaker was kept in a muffle furnace at an initiating combustion temperature of 500±20 °C for the burning process. After all the liquid had evaporated, the reagents decomposed and released large amounts of gasses. A large amount of heat released (due to the exothermic nature of this process) resulted in a flame that decomposed the reagents further and released more gasses. The flame lasted for ~60 seconds and the combustion process was completed within 5 minutes. The resulting white foamy and voluminous combustion products were cooled down to room temperature. This foamy mass was ground gently using a pestle and mortar to get a fine powder. $LaMgAl_{11}O_{19}$: Tb, Sm powder yield to a composition with the general formula $LaMgAl_{11}O_{19}$: 0.02Tb, ySm (y = 0.5, 1, 1.5, 2) for different concentrations of Sm^{3+}. This powder was then used for the further characterizations.

Characterizations

The phase composition and phase structure were measured by X-ray diffraction (XRD) pattern. XRD performed with P-analytical diffractometer with Cu Kα radiation (λ=1.5405 A°) operating at 40kV, 30mA anode current, was used to identify the major phases of the powders. These were compared to the JCPDS card for $LaMgAl_{11}O_{19}$. The XRD data were collected in a 2θ range from 10 to 80°, with the continuous scan mode. The morphology and microstructure were characterized with JEOL, JSM-6360LV SEM environmental scanning electron microscope (SEM). The PL excitation and emission spectra were recorded using a RF-5301PC Spectrofluorophotometer fitted with a sensitive photomultiplier tube with a 150W 'xenon flash lamp' as an excitation source. The excitation and emission spectra were recorded using a spectral slit width of 1.5 nm with high sensitivity. All the measurements were carried out at room temperature.

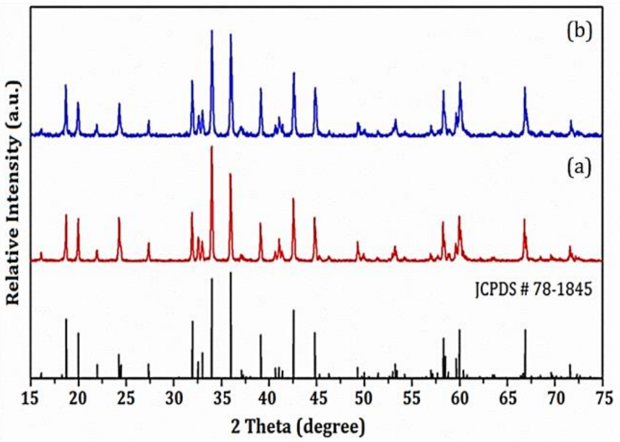

Fig. 1. XRD patterns of (a) pure and (b) Tb^{3+}/Sm^{3+} co-doped LMA phosphors along with standard JCPDS card no. 78-1845.

Results and discussion

Phase analysis and morphology

The phase purity of prepared samples is checked by XRD patterns. The XRD patterns of pure and Tb^{3+}/Sm^{3+} co-doped LMA phosphors along with the standard JCPDS card no. 78-1845 are shown in **Fig. 1**. Both the XRD patterns show well-defined peaks, which reveals the crystallinity and phase formation of the synthesized compounds. The samples exhibit identical diffraction patterns as the standard JCPDS card and confirm that the samples are of the hexagonal structure with space group $P6_{3/}mmc$ (194). In the XRD pattern, there is no significant influence on the host lattice by the incorporation of a small amount of dopant ions as there are no extra peaks related to the second phase which suggests that the dopant ions completely incorporated to the host. The crystal size is evaluated using the Debye-Scherer's equation. The average crystal size for prepared sample is found to be in the range of 180-200 nm. **Fig. 2(a-b)** exhibits the SEM micrographs for LMA: Tb^{3+}, Sm^{3+} phosphors at different magnification levels. Reaction in the presence of urea allows the varying size and shape of particles. This irregularity in size and shapes of particles is caused by the non-uniform distribution of temperature and irregular mass flow during combustion process.

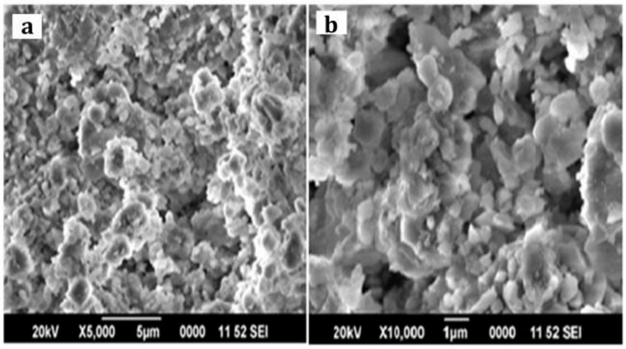

Fig. 2. SEM images of LMA: $2Tb^{3+}/1.5Sm^{3+}$ phosphor.

Optical properties of Tb^{3+} and Sm^{3+} doped LMA

Fig. 3(a) depicts the PL excitation (PLE) spectrum of LMA: Tb^{3+} (2 mol%) phosphor by monitoring emission wavelength of 545 nm. The spectrum consists of a broad band ranging from 240 to 280 nm with the maximum at 260 nm, corresponding to $4f^8 \rightarrow 4f^7 5d^1$ transition of Tb^{3+} and a series of spectral bands in the range of 300–400 nm, analogous to the transitions between 4f→4f states of Tb^{3+} [**14,22**]. The f→f transitions of Tb^{3+} have been properly designated as $^7F_6 \rightarrow {}^5H_7$ at 317 nm, $^7F_6 \rightarrow {}^5D_2$ at 350 nm and 358 nm, and $^7F_6 \rightarrow {}^5G_6$ at 375 nm [**23**]. PL emission spectra of LMA: Tb^{3+} phosphor with different concentration of Tb^{3+} under the excitation of 260 nm are shown in **Fig. 3(b)**. The PL spectra consist of a series of sharp lines in the 480-600 nm regions. The emission bands at 489, 545, and 571 nm can be attributed to the $^5D_4 \rightarrow {}^7F_6$, $^5D_4 \rightarrow {}^7F_5$, and $^5D_4 \rightarrow {}^7F_4$ transitions of Tb^{3+}, respectively. Among them, the transition of $^5D_4 \rightarrow {}^7F_5$ with green emission at 545 nm is predominant, which can be described by the large values of the reduced matrix elements at J = 5 and the Judd–Ofelt theory [**24,25**]. The relative intensity of Tb^{3+} (545 nm) emissions as functions of Tb^{3+} concentration for LMA: Tb^{3+} phosphors are shown in the inset of **Fig. 3(b)**. It is found that the relative emission intensity of Tb^{3+} at 545 nm initially increases up to 2 mol% and then decreases when Tb^{3+} concentration further increases. Hence the optimal doping concentration has been found that about 2 mol%.

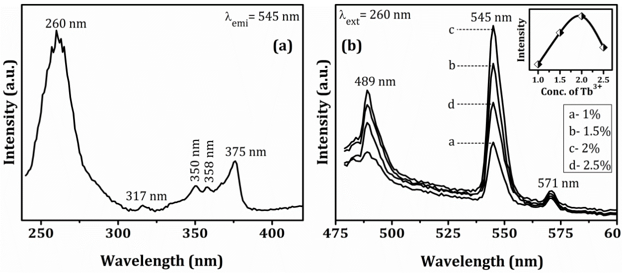

Fig. 3. (a) PL excitation (PLE) spectrum of LMA: $0.02Tb^{3+}$ phosphor. (b) PL spectra of LMA: Tb^{3+} phosphors. Inset shows dependence of emission intensity on content of Tb^{3+} in LMA: Tb^{3+} phosphors.

In **Fig. 4(a)**, the PLE spectrum of LMA: Sm^{3+} (1.5 mol%) phosphor (monitored at 602 nm) shows several peaks, which are located at 343, 360, 375, 403, 417, 438, 462, and 470 nm. These excitation lines are corresponding to the electronic transitions of $^6H_{5/2} \rightarrow {}^4K_{15/2}$, $^6H_{5/2} \rightarrow {}^4D_{3/2}$, $^6H_{5/2} \rightarrow {}^6P_{7/2}$, $^6H_{5/2} \rightarrow {}^4F_{7/2}$, $^6H_{5/2} \rightarrow {}^6P_{5/2}$, $^6H_{5/2} \rightarrow {}^4G_{9/2}$, $^6H_{5/2} \rightarrow {}^4I_{9/2}$, and $^6H_{5/2} \rightarrow {}^4I_{13/2}$, respectively [**26**]. Among all these peaks, the strongest one belongs to the $^6H_{5/2} \rightarrow {}^4F_{7/2}$ transition at 403 nm in the range of n-UV wavelength, which makes LMA: Sm^{3+} phosphors suitable for white lighting devices based on GaN LEDs. Figure 4(b) depicts the PL emission spectra of LMA: Sm^{3+} phosphors by monitoring emission wavelength at 403 nm. It consists of four characteristic emission peaks at 566, 603, 651, and 707 nm which are assigned to $^4G_{5/2} \rightarrow {}^6H_{5/2}$, $^4G_{5/2} \rightarrow {}^6H_{7/2}$, $^4G_{5/2} \rightarrow {}^6H_{9/2}$, and $^4G_{5/2} \rightarrow {}^6H_{11/2}$ transitions of Sm^{3+}, respectively. Among these emission peaks, the transition at 603 nm ($^4G_{5/2} \rightarrow {}^6H_{7/2}$) had the maximum intensity than other three transitions, which corresponds to red emission of LMA: Sm^{3+} phosphors. The selection rule $\Delta J = \pm 1$, (where J = angular momentum) satisfied by strongest transition $^4G_{5/2} \rightarrow {}^6H_{7/2}$ (603 nm) which reveals it is a partly magnetic dipole (MD) and partly electric dipole (ED) natured. Furthermore, the peak at 566 nm ($^4G_{5/2} \rightarrow {}^6H_{5/2}$) is MD transition natured and another peak at 651 nm ($^4G_{5/2} \rightarrow {}^6H_{9/2}$) is purely ED transition natured, which is very sensitive to the crystal field. Frequently, to recognize the symmetry of the surrounding environment of the trivalent 4f ions, intensity ratio ED/MD can be used, which can be related to the site symmetry around the Sm^{3+} ions in the host matrix. When the ED transition is more intense than the MD transition then asymmetric nature is dominated [**27**]. In the present work, the emission intensity of $^4G_{5/2} \rightarrow {}^6H_{5/2}$ (MD) transition is higher than that of $^4G_{5/2} \rightarrow {}^6H_{9/2}$ (ED) transition, indicating the symmetric nature of Sm^{3+} ions in LMA host matrix. Inset of **Fig. 4(b)** shows the dependence of emission intensity on the content of Sm^{3+} in LMA: Sm^{3+} phosphors. The maximum emission intensity is observed at 1.5 mol% concentration of Sm^{3+} ions.

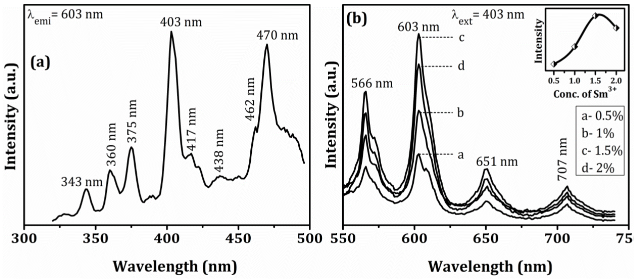

Fig. 4. (a) PLE spectrum of LMA: $0.015Sm^{3+}$. (b) PL emission spectra of LMA: Sm^{3+}.
Inset shows dependence of emission intensity on content of Sm^{3+} in LMA: Sm^{3+} phosphors.

Energy transfer mechanism in LMA: Tb^{3+}, Sm^{3+}

Figure 5(a) depicts the comparison of PLE spectra of Tb^{3+} and Sm^{3+} ions individually and co-doped LMA phosphors by monitoring the Tb^{3+} (545 nm) and Sm^{3+} (603 nm) emission wavelengths. The excitation spectra of Tb^{3+} and Tb^{3+}/Sm^{3+} doped LMA phosphors by monitoring the Tb^{3+}

emission wavelength at 545 nm shows similar excitation peaks with strong broadband due to $4f^8 \rightarrow 4f^7 5d$ transition of Tb^{3+} centered at 260 nm in the lower wavelength region and weak f→f transitions of Tb^{3+} ions in the wavelength range of 300–380 nm without any Sm^{3+} excitation peaks (in Tb^{3+}/Sm^{3+} ions co-doped sample), as can be seen in the **Fig. 5(a)** [(i) & (iii)]. The only Sm^{3+} doped LMA phosphor excited at 603 nm exhibits strong f→f transitions in the lower energy side as shown in **Fig. 5(a)** [(ii)]. Similarly, when the PLE spectra of LMA:Tb^{3+}/Sm^{3+} phosphor are monitored at 603 nm (Sm^{3+} emission wavelength), strong f→d transition bands of Tb^{3+} ions in the higher energy region and strong f→f transitions bands of Sm^{3+} ions in the lower energy region are seen as shown in **Fig. 5(a)**[(iv)] [**28**]. All the excitation spectra of LMA phosphor at different emission wavelengths showed the common excitation band at 375 nm attributable to $^7F_6 \rightarrow {}^5G_6$ of Tb^{3+} ion and $^6H_{5/2} \rightarrow {}^6P_{7/2}$ of Sm^{3+} ion [**29**].

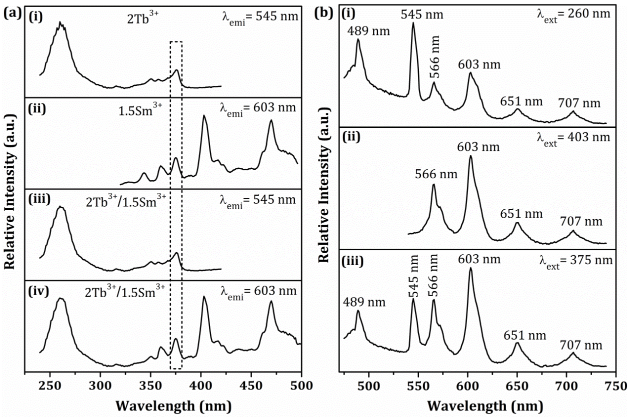

Fig. 5. (a) PLE spectra of $2Tb^{3+}$, $1.5Sm^{3+}$ and $2Tb^{3+}/1.5Sm^{3+}$ doped LMA phosphors by monitoring the emission wavelengths of 545 and 603 nm (the highlighted line shows the common excitation peak). (b) PL spectra of $2Tb^{3+}/1.5Sm^{3+}$ doped LMA phosphor at the excitation wavelengths of 260, 403 and 375 nm.

Fig. 5(b) depicts the PL spectra of LMA: $0.02Tb^{3+}/0.015Sm^{3+}$ phosphor obtained at excitation wavelengths of 260, 403, and 375 nm. The LMA: $0.02Tb^{3+}/0.015Sm^{3+}$ phosphor shows the green emission bands of Tb^{3+} ions including weak Sm^{3+} transitions obtained upon excitation at 260 nm wavelengths. Only Sm^{3+} emission bands without Tb^{3+} emission at 566, 603, 651, and 707 nm due to $^4G_{5/2} \rightarrow {}^6H_{5/2}$, $^4G_{5/2} \rightarrow {}^6H_{7/2}$, $^4G_{5/2} \rightarrow {}^6H_{9/2}$, and $^4G_{5/2} \rightarrow {}^6H_{11/2}$ transitions, respectively, are observed upon excitation at 403 nm wavelengths. It is caused by the overlapping of the Sm^{3+} ($^6G_{5/2} \rightarrow {}^6H_{7/2}$) emission with the tail of Tb^{3+} ($^5D_4 \rightarrow {}^7F_4$) emission. However, the common excitation wavelength of 375 nm can be found for LMA: Tb^{3+}/Sm^{3+} phosphors. At the common excitation of 375 nm, PL spectra shows three groups of emission bands blue region related to the electronic transitions $^5D_3 \rightarrow {}^7F_J$ (J = 5, 4, 3, and 2), green region $^5D_4 \rightarrow {}^7F_J$ (J = 6, 5, and 4) of Tb^{3+}, and orange-red region $^4G_{5/2} \rightarrow {}^6H_{J/2}$ (J = 5, 7, 9, and 11) transitions of Sm^{3+}, respectively due to the ET from Tb^{3+} to Sm^{3+} ions. As compared to the blue emission, the green emission was dominant in the emission spectrum, so we observed only the green emission with the naked eye.

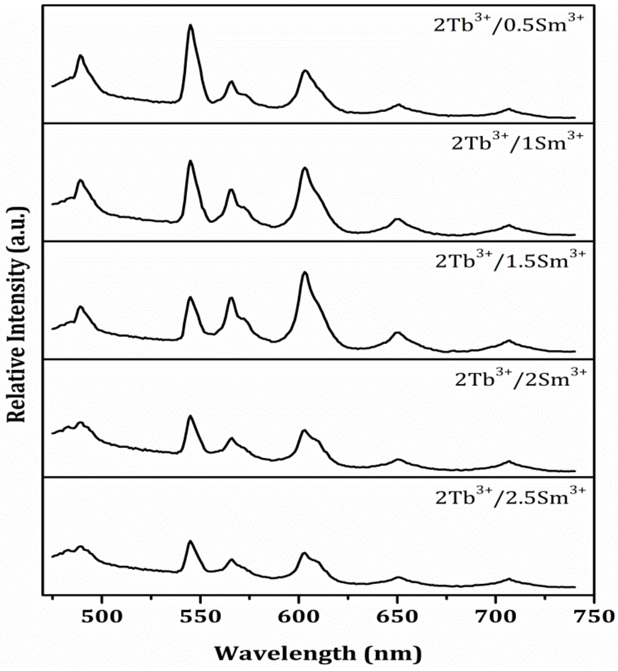

Fig. 6. PL spectra of LMA: $2Tb^{3+}/Sm^{3+}$ at different concetrations of Sm^{3+} ions under 375 nm common excitation.

Fig. 6 depicts the PL spectra of the LMA: $2Tb^{3+}/Sm^{3+}$ samples with different concentrations of Sm^{3+} under common excitation at 375 nm. It can be seen that with increasing Sm^{3+} concentration, the emission intensity of Tb^{3+} ions reduces while it is of Sm^{3+} ion enhances due to the efficient ET from Tb^{3+} to Sm^{3+} ions. It reveals that the Sm^{3+} ions sensitized by Tb^{3+} ions through ET and the energy is transferred from Tb^{3+} to Sm^{3+}. However, it is clear that, upon increasing the Sm^{3+} content above 1.5 mol%, the intensities of the Sm^{3+} emission begin to reduce as a result of a self-quenching effect (SQE) due to the interactions between Sm^{3+} ions [**30**]. **Fig. 7(a)** depicts the dependence of emission intensities of Tb^{3+} at 545 nm, Sm^{3+} at 603 nm and ET efficiency of $Tb^{3+} \rightarrow Sm^{3+}$ as a function of Sm^{3+} concentrations.

The ET efficiency (η_T) from sensitizer Tb^{3+} to activator Sm^{3+} in LMA: Tb^{3+}/Sm^{3+} samples can be approximately evaluate according to the data of intensity by using fallowing formula.

$$\eta_T = 1 - [I_s/I_{s0}] \tag{1}$$

where I_s and I_{so} are the luminescence intensity of sensitizer Tb^{3+} ions in the presence and absence of activator Sm^{3+} ions, respectively. The evaluate ET efficiency for different concentrations of Sm^{3+} ions were 30% (0.5 mol%), 52.1% (1 mol%), 62.19% (1.5 mol%), 69.23% (2 mol%), and 78.28% (2.5 mol%). It can be seen that the ET efficiency increases with increasing Sm^{3+}

concentration, and reaches 78.28% at 2.5 mol%, demonstrating that the ET from Tb^{3+} to Sm^{3+} is efficient. Moreover, the critical distance (R_c) in LMA: Tb^{3+}/Sm^{3+} phosphor also can be estimated through the formula suggested by Blasse [**31**],

$$R_c \approx 2\left[\frac{3V}{4\pi X_c N}\right]^{1/3} \tag{2}$$

where V is the volume of the unit cell, X_c is the critical concentration, and N represents the number of Z ions in the unit cell. For LMA host, V = 686.21 Å^3, N = 2 and X_c is the sum content of Tb^{3+} and Sm^{3+} ions, at which the luminescence intensity of Tb^{3+} ions is half of that in the absence of Sm^{3+} and found to be 0.03 mol from the **Fig. 7(a)**. The critical distance (R_c) is estimated to be about 27.96 Å. Since the value of R_c is much longer than 5 Å, this implies that the exchange interaction would not be responsible for the ET mechanism from Tb^{3+} to Sm^{3+} ions. Consequently, only electric multipolar interactions contribute to the ET mechanism in this case. To understand the multipolar interactions, fallowing relationship can be obtained [**32**],

$$\frac{I_{so}}{I_s} \propto C^{n/3} \tag{3}$$

where I_s and I_{so} are the luminescence intensity of sensitizer Tb^{3+} ions in the presence and absence of activator Sm^{3+} ions, respectively. C is the total concentration of Tb^{3+} and Sm^{3+} ions. The relationships between I_{so}/I_s and $C^{n/3}$ based on the Eq. (3) are illustrated in **Fig. 7(b)**. The linear behavior was observed only when n = 6, indicating that the ET from Tb^{3+} to Sm^{3+} ions in LMA: Tb^{3+}/Sm^{3+} phosphor takes place through the dipole–dipole interactions mechanism. All results suggest that Tb^{3+} ions act as a sensitizer when co-doped with Sm^{3+} ions and also such combination of dual RE ions doped optical materials find potential applications as multicolor emitting phosphor.

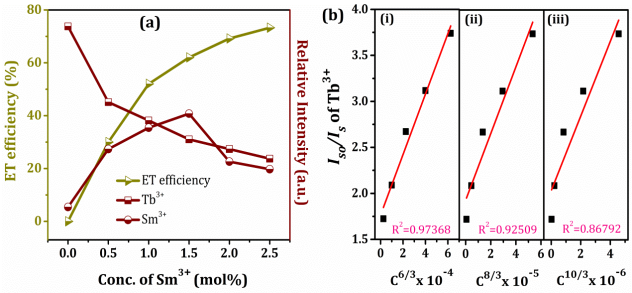

Fig. 7. (a) Dependence of the emission intensity of Tb^{3+}, Sm^{3+} ions and ET efficiency on the Sm^{3+} concentration in LMA:Tb^{3+}/Sm^{3+} phosphors. (b) Dependence of $\boldsymbol{I_{so}/I_s}$ of Tb^{3+} on (i) $C^{6/3}$, (ii) $C^{8/3}$, (iii) $C^{10/3}$, respectively.

Conclusions

A series of Tb^{3+}/Sm^{3+} single as well as co-doped LMA phosphors with tetragonal structure were successfully synthesized by using low-temperature solution combustion technique. The critical distance (R_c) has been calculated by the concentration quenching method and it is found to be 27.96 Å. The ET efficiency also has been calculated, it increases with increasing Sm^{3+} doping content, and its value was estimated to be 78.28% when the content of Sm^{3+} was up to 2.5 mol%. This shows efficient ET from Tb^{3+} to Sm^{3+} in LMA: Tb^{3+}/Sm^{3+} phosphor. LMA: Tb^{3+}/Sm^{3+} phosphor exhibited great potential applications as multicolor emitting phosphor for solid-state lighting.

Acknowledgement

Author SPP is thankful to management of the Institution KNM, Nagpur for providing useful facilities of the instrumentation, SHIMADZU Spectro fluorophotometer (RF-5301 PC).

Keywords

$LaMgAl_{11}O_{19}$, luminescence, energy transfer, dipole-dipole interaction, concentration quenching.

Received: 22 May 2020
Revised: 22 July 2020
Accepted: 01 September 2020

References

1. Blasse G, Grabmaier BC. Luminescent Material. Springer-Verlag. Berlin Heidelberg New York London Paris Tokyo Hong Kong Barcelona Budapest: Springer-Verlag Berlin Heidelberg New York; **1994**. 1-232.
2. Li, B.; Sun, Q.; Wang, S.; Guo, H.; Huang, X.; *RSC Adv*., **2018**, *8*, 9879.
3. Guan, H.; Liu, G.; Wang, J.; Dong, X.; Yu, W.; *Dalt Trans*., **2014**, *43*, 10801.
4. Zhou, J.; Xia, Z.; *J. Mater Chem. C*., **2014**, *2*, 6978.
5. Liu, T.; Meng, Q.; Sun, W.; *J. Lumin*., **2016**, *170*, 219.
6. Mendhe, M.S.; Puppalwar, S.P.; Dhoble, S.J.; *Luminescence: Journal of Bio and Chem Luminescence*, **2016**, *31*, 881.
7. Premkumar, H.B.; Sunitha, D.V.; Singh, F.; Nagabhushana, H.; Sharma, S.C.; Nagabhushana, B.M.; et al. *J. Lumin*., **2012**, *132*, 2679.
8. Yang, C.; Liu, Q.; Huang, D.; Li, X.; Zhang, X.; Bai, Z.; Wang, X.; Mia, X.; *J. Lumin*., **2019**, *214*, 116541.
9. Li, Z.; Zhong, B.; Cao, Y.; Zhang, S.; Lu, Y.; Mu, Z.; Hu, Z.; Hu, Y.; *J. Mater. Science: Mater. Electronics*., **2019**, *30*, 10491.
10. Yang, C.; Li, X.; Liu, Q.; Xang, X.; Bai, X.; Wang, X.; Mi, X.; *J. Mater. Science: Mater. Electronics*, **2020**, *31*, 1057.
11. Suchithra, V.G.; Rao, P.P.; Aswathy, B.A.; *J. Mater. Science: Mater. Electronics*, **2020**, *31*, 5141.
12. Kumar, K.A.; Babu, S.; Prasad, V.R.; Damodaraiah, S.; Ratnakaram, Y.C.; *Mater. Res. Bull*., **2017**, *90*, 31.
13. Li, K.; Shang, M.; Lian, H.; Lin, J.; *J. Mater. Chem. C*., **2016**, *4*, 5507.
14. Mendhe, M.S.; Puppalwar, S.P.; Dhoble, S.J.; *Optik*, **2018,** *166*, 15.
15. Mendhe, M.S.; Puppalwar, S.P.; Dhoble, S.J.; *Optical Materials*, **2018**, *82*, 47.
16. Sheng, T.; Fu, Z.; Wang, X.; Zhou, S.; Zhang, S.; Dai, Z.; *J. Phys. Chem. C*., **2012**, *116*, 19597.
17. Reddy, C.P.; Naresh, V.; Ramaraghavulu, R.; Rudramadevi, B.H.; Reddy, K.T.R.; Buddhudu, S.; *Spectrochim ACTA PART A Mol Biomol Spectrosc*., **2015**, *144*, 68.
18. Liu, H.; Liao, L.; Chen, J.; Guo, Q.; Zhang, Y.; Mei, L.; *J. Lumin*., *Elsevier*, **2016**, *169*, 739.
19. Min, X.; Fang, M.; Huang, Z.; Liu, Y.; Tang, C.; Zhu, H.;, et al. *Opt Mater*., **2014**, *37*, 110.
20. Min, X.; Huang, Z.; Fang, M.; Liu, Y.; Tang, C.; Wu, X.; *Inorg Chem*., **2014,** *53*, 6060.
21. Ballesteros, C.; Gonza´ lez R.; Chen, Y.; Kokta, M.R.; *Phys. Rev. B: Condens. Matter*., **1993**, *47*, 2460.
22. Sun, J.; Sun, Y.; Lai, J.; Xia, Z.; Du, H.; *J. Lumin*., **2012**, *132*, 3048.
23. Naresh, V.; Buddhudu, S.; *J. Lumin*., **2013**, *137*, 15.
24. Wen, Y.; Wang, Y.H.; Zhang, F.; Liu, B.T.; *Mater Chem Phys. B.V.*; **2011**, *129*, 1171.

25. Rao, V.; Kumar, B.; Jayasimhadri, M.; Jang, K.; Lee, H.; Yi, S.; et al. *J. Cryst Growth*, **2011**, *326*, 120.
26. Gupta, S.K.; Pathak, N.; Thulasidas, S.K.; Natarajan, V.*; J. Lumin*., **2016**, *169*, 669.
27. Gupta, S.K.; Ghosh, P.S.; Pathak, N.; Arya, A.; Natarajana, V.; *RSC Adv*., **2014**, *4*, 29202.
28. Pavitra, E.; Raju, GSR.; Ko, Y.H.; Yu, J.S.; *Phys. Chem. Chem Phys*., **2012**, *14*, 11296.
29. Jeon, Y.; Bharat, L.K.; Yu, J.S.; *J. Lumin*., **2015**, *166*, 93.
30. Lakshminarayana, G.; Yang, R.; Qiu, J.R.; Brik, M.G.; Kumar, G.A.; Kityk, I.V.; *J. Phys. D Appl Phys*., **2009**, *42*, 015414.
31. Blasse, G.; *Philips Res Rep*., **1969**, *24*, 131.
32. Dexter, D.L.; Schulman, J.H.; *J. Chem Phys*., **1954**, *22*, 1063.

Authors biography

Dr. Suresh Puppalwar obtained M.Sc. and Ph.D. degree in Physics from RTM Nagpur University, Nagpur, India. He is presently working as Associate Professor in Department of Physics, Kamla Nehru Mahavidyalaya, Nagpur, India. His research of interest is synthesis and characterization of luminescent materials for solid state lighting and development of TLD phosphors for radiation dosimetry. He is an active member of Luminescence Society of India. He is also a member of IAAM.

Dr. Mukesh Mendhe has done his M.Sc. and Ph.D. degree from Department of Physics, Kamla Nehru Mahavidyalaya, Nagpur, affiliated to RTM Nagpur University, Nagpur. His research work is on energy transfer in luminescent materials applied for solid state lighting.

Dr. S.J. Dhoble is currently working as a Professor in the Department of Physics, R.T.M. Nagpur University, Nagpur-India. Prof. Dhoble published more than 500 research papers in peer reviewed journals on solid-state lighting, LEDs, radiation dosimetry and laser materials and has one international patent. He is author of 23 books/ Chapters. He received Outstanding Scientist-2015 award in outstanding research contribution in Solid State Physics at Chennai from Venus International Foundation. He is the Editor of Luminescence: The Journal of Biological and Chemical Luminescence, John Wiley & Sons Ltd.